Automated multi-parameter measurement of cardiomyocytes dynamics with digital holographic microscopy

Benjamin Rappaz,[1] Inkyu Moon,[2,*] Faliu Yi,[2] Bahram Javidi,[3] Pierre Marquet,[4,5,†] and Gerardo Turcatti,[1,†]

[1]*Biomolecular Screening Facility (BSF), Ecole Polytechnique Fédérale de Lausanne (EPFL), Lausanne, Switzerland*
[2]*Dept. of Computer Engineering, Chosun University, 309 Pilmun-daero, Dong-gu, Gwangju, 501-759 South Korea*
[3]*Dept. of Electrical and Computer Engineering, U-2157, University of Connecticut, Storrs, Connecticut, 06269 USA*
[4]*LNDC, BMI, Ecole Polytechnique Fédérale de Lausanne (EPFL), Lausanne, Switzerland*
[5]*Centre de Neurosciences Psychiatriques, Département de psychiatrie DPCHUV, Prilly Lausanne, Switzerland*
[†]*co-last authors*
[*]*inkyu.moon@chosun.ac.kr*

Abstract: Compounds tested during drug development may have adverse effects on the heart; therefore all new chemical entities have to undergo extensive preclinical assessment for cardiac liability. Conventional intensity-based imaging techniques are not robust enough to provide detailed information for cell structure and the captured images result in low-contrast, especially to cell with semi-transparent or transparent feature, which would affect the cell analysis. In this paper we show, for the first time, that digital holographic microscopy (DHM) integrated with information processing algorithms automatically provide dynamic quantitative phase profiles of beating cardiomyocytes. We experimentally demonstrate that relevant parameters of cardiomyocytes can be obtained by our automated algorithm based on DHM phase signal analysis and used to characterize the physiological state of resting cardiomyocytes. Our study opens the possibility of automated quantitative analysis of cardiomyocyte dynamics suitable for further drug safety testing and compounds selection as a new paradigm in drug toxicity screens.

OCIS codes: (090.1995) Digital holography; (100.6890) Three-dimensional image processing; (170.3880) Medical and biological imaging; (170.1530) Cell analysis; (999.9999) Quantitative phase microscopy; (999.9999) Cardiomyocyte; (999.9999) Cardiotoxicity; (999.9999) High content screening.

References and links

1. J. Dykens, Y. Will, "The significance of mitochondrial toxicity testing in drug development," Drug discovery today **12**(17), 777-785 (2007).
2. B. Xi, T. Wang, and N. Li, "Functional cardiotoxicity profiling and screening using the xCELLigence RTCA Cardio System," Journal of the Association for Laboratory Automation **16**(6), 415-421 (2011).
3. O. Sirenko, C. Crittenden, and N. Callamaras, "Multiparameter in vitro assessment of compound effects on cardiomyocyte physiology using iPSC cells," Journal of biomolecular screening **18**(1), 39-53 (2013).
4. S. Braam, L. Tertoolen, and A. Stolpe, "Prediction of drug-induced cardiotoxicity using human embryonic stem cell-derived cardiomyocytes," Stem cell research **4**(2), 107-116 (2010).
5. M. Jonsson, Q. Wang, and B. Becker, "Impedance-based detection of beating rhythm and proarrhythmic effects of compounds on stem cell-derived cardiomyocytes," Assay and drug development technologies **9**(6), 589-599 (2011).
6. N. Shaked, L. Satterwhite, and N. Bursac, "Whole-cell-analysis of live cardiomyocytes using wide-field interferometric phase microscopy," Biomedical optics express **1**(2) 706-719 (2010).
7. Y. Abassi, B. Xi, N. Li, W. Ouyang, A. Seiler, M. Watzele, R. Kettenhofen, H. Bohlen, A. Ehlich, E. Kolossov, X. Wang, and X. Xu, "Dynamic monitoring of beating periodicity of stem cell-derived

cardiomyocytes as a predictive tool for preclinical safety assessment," British journal of pharmacology **165**(5), 1424-1441 (2012).

8. C. Carlson, C. Koonce, N. Aoyama, S. Einhorn, S. Fiene, A. Thompson, B. Swanson, B. Anson, and S. Kattman, "Phenotypic screening with human iPS Cell-Derived Cardiomyocytes HTS-Compatible Assays for Interrogating Cardiac Hypertrophy," Journal of biomolecular screening **18**(10), 1203-1211 (2013).
9. O. Sirenko, E. F. Cromwell, C. Crittenden, J. Wignall, F. Wright, I. Rusyn, "Assessment of beating parameters in human induced pluripotent stem cells enables quantitative in vitro screening for cardiotoxicity," Toxicology and applied pharmacology **273**(3), 500-507 (2013).
10. R. Yuste, "Fluorescence microscopy today, Nature methods," **2**(12), 902-904 (2005).
11. D. Stephens and V. Allan, "Light microscopy techniques for live cell imaging," Science **300**(5616), 82-86 (2003).
12. V. Salnikov, Y. Lukyanenko, W. Lederer, and V. Lukyanenko, "Distribution of ryanodine receptors in rat ventricular myocytes," J. Muscle Res. Cell Motil. **30**(3-4), 161-170 (2009).
13. D. Hickson-Bick, G. Sparagna, L. Buja, and J. McMillin, "Palmitate-induced apoptosis in neonatal cardiomyocytes is not dependent on the generation of ROS," Am. J. Physiol. Heart Circ. Physiol. **282**(2), H656-H664 (2002).
14. M. Sarah and B. Antony, "Preparation of plant cells for transmission electron microscopy to optimize immunogold labeling of carbohydrate and protein epitopes," Nature protocols **7**, 1716-1727 (2012).
15. W. Moerner and D. Fromm, "Methods of single-molecule fluorescence spectroscopy and microscopy," Review of Scientific Instruments **74**(8), 3597-3619 (2003).
16. D. Alsteens, H. Trabelsi, P. Soumillion, and Y. Dufrêne, "Multiparametric atomic force microscopy imaging of single bacteriophages extruding from living bacteria," Nature communications **4**, 2926 (2013).
17. E. Azeloglu and K. Costa, "Cross-bridge cycling gives rise to spatiotemporal heterogeneity of dynamic subcellular mechanics in cardiac myocytes probed with atomic force microscopy," Am. J. Physiol. Heart Circ. Physiol. **298**(3), H853-H860 (2010).
18. A. Kamgoue, J. Ohayon, Y. Usson, L. Riou, and P. Tracqui, "Quantification of cardiomyocyte contraction based on image correlation analysis," Cytometry A **75**(4), 298-308 (2009).
19. N. Pavillon, A. Benke, D. Boss, C. Moratal, J. Kühn, P. Jourdain, C. Depeursinge, P. Magistretti, and P. Marquet, "Cell morphology and intracellular ionic homeostasis explored with a multimodal approach combining epifluorescence and digital holographic microscopy," Journal of biophotonics **3**(7), 432-436 (2010).
20. P. Marquet, B. Rappaz, P. Magistretti, E. Cuche, Y. Emery, T. Colomb, and C. Depeursinge, "Digital holographic microscopy: a noninvasive contrast imaging technique allowing quantitative visualization of living cells with subwavelength axial accuracy," Optics letters **30**(5), 468-470 (2005).
21. Y. Cotte, F. Toy, P. Jourdain, N. Pavillon, D. Boss, P. Magistretti, P. Marquet, and C. Depeursinge, "Marker-free phase nanoscopy," Nature Photonics **7**(2), 113-117 (2013).
22. I. Moon, M. Daneshpanah, B. Javidi, and A. Stern, "Automated three-dimensional identification and tracking of micro/nanobiological organisms by computational holographic microscopy," Proc. IEEE **97**(6), 990-1010 (2009).
23. P. Ferraro, S. Grilli, D. Alfieri, S. Nicola, and A. Finizio, 2005. "Extended focused image in microscopy by digital Holography," Opt Express **13** 6738-6749 (2005).
24. B. Xi, T. Wang, N. Li, W. Ouyang, W. Zhang, J. Wu, X. Xu, X. Wang, and Y. Abassi, "Functional cardiotoxicity profiling and screening using the xCELLigence RTCA Cardio System," Journal of the Association for laboratory automation **16**(6), 415-421 (2011).
25. F. Yi, I. Moon, and Y. Lee, "Three-dimensional counting of morphologically normal human red blood cells via digital holographic microscopy," Journal of biomedical optics **20**(1), 016005 (2015).
26. A. Mallahi, C. Minetti, and F. Dubois, "Automated three-dimensional detection and classification of living organisms using digital holographic microscopy with partial spatial coherent source: application to the monitoring of drinking water resources," Appl. Optics **52**, A62-A80 (2013).
27. I. Moon, B. Javidi, F. Yi, D. Boss, and P. Marquet, "Automated statistical quantification of three-dimensional morphology and mean corpuscular hemoglobin of multiple red blood cells," Opt. Express **20**, 10295-10309 (2012).
28. P. Langehanenberg, L. Ivanova, I. Bernhardt, S. Ketelhut, A. Vollmer, D. Dirksen, G. Georgiev, G. Bally, B. Kemper, "Automated three-dimensional tracking of living cells by digital holographic microscopy," J. Biomed. Opt. **14**(1), 014018 (2009).
29. J. Kuhn, E. Shaffer, J. Mena, B. Breton, J. Parent, B. Rappaz, M. Chambon, Y. Emery, P. Magistretti, C. Depeursinge, P. Marquet, and G. Turcatti, "Label-free cytotoxicity screening assay by digital holographic microscopy," Assay and drug development technologies **11**(2), 101-107 (2013).
30. B. Rappaz, B. Breton, E. Shaffer, and G. Turcatti, "Digital holographic microscopy: a quantitative label-free microscopy technique for phenotypic screening," Combinatorial chemistry & high throughput screening **14**(1), 80-88 (2014).

31. C. Hsieh, R. Grange, Y. Pu, and D. Psaltis, "Three-dimensional harmonic holographic microcopy using nanoparticles as probes for cell imaging," Opt Express **17**, 2880-2891 (2009).
32. F. Dubois, C. Yourassowsky, O. Monnom, J. Legros, and O. Debeir, "Digital holographic microscopy for the three-dimensional dynamic analysis of in vitro cancer cell migration," J. Biomed. Opt. **11**(5), 054032 (2006).
33. R. Barer, "Determination of dry mass, thickness, solid and water concentration in living cells," Nature **172**, 1097-1098 (1953).
34. B. Rappaz, E. Cano, T. Colomb, J. Kuhn, C. Depeursinge, V. Simanis, P. Magistretti, and P. Marquet, "Noninvasive characterization of the fission yeast cell cycle by monitoring dry mass with digital holographic microscopy," Journal of biomedical optics **14**(3), 034045-034049 (2009).
35. D. Boss, J. Kuhn, P. Jourdain, C. Depeursinge, P. Magistretti, and P. Marquet, "Measurement of absolute cell volume, osmotic membrane water permeability, and refractive index of transmembrane water and solute flux by digital holographic microscopy," J. Biomed. Opt. **18**, 036007 (2013).
36. B. Rappaz, A. Barbul, Y. Emery, R. Korenstein, C. Depeursinge, P. Magistretti, and P. Marquet, "Comparative study of human erythrocytes by digital holographic microscopy, confocal microscopy, and impedance volume analyzer," Cytometry Part A **73**(10), 895-903 (2008).
37. R. Gonzalez and R. Woods, *Digital Imaging Processing* (Prentice Hall, New York, 2002).

1. Introduction

During the lengthy drug discovery process, it is crucial to improve the predictability of compound toxicity through safety profiling assays. This is done in order to detect potentially toxic compounds early in the process before significant time and important financial investments are made. Between 1994 and 2006, 38 of the new drugs approved by the US Food and Drug Administration (FDA) were later withdrawn from the market because of safety concerns, the majority being cardiotoxic or hepatotoxic [1]. Safety assessments are therefore performed in preclinical drug development for revealing possible drug side effects in particular those that may affect the electrical conduction and beating of the heart [2-6]. Therefore, researchers and pharmaceutical companies have to ensure that the effect of lead candidate compounds on cardiac function strictly satisfy safety criteria. Consequently, it is critical to establish more informative in vitro cardiotoxicity screens and data analysis algorithms at the early phases of drug development for preventing late stage failure [7-9].

Cardiomyocytes or myocardial cells are the main contractile elements of the heart muscle. These cells work cooperatively to generate human heart beating and control blood flow through the blood vessels of the circulatory system [6]. Like many other types of biological cells, cardiomyocytes are mostly transparent. As a result, conventional two-dimensional (2D) imaging systems based solely on the intensity of bright-field only generate a low contrast captured image with limited informative details on the cell structure. Even though some optical imaging techniques, such as phase contrast and differential interference contrast microscopies, can generate contrast from transparent cells, they cannot provide quantitative information about their thickness.

Various imaging systems have been previously used to study cardiomyocytes. For instance with fluorescence microscopy [10-11], specific biological molecules can be fluorescently stained and the location of a protein can be traced or the activity of a specific ions can be monitored in time [12-13]. However fluorescence can fade or interfere with the measured molecule [14-15]. Atomic force microscopy [16] allows measuring advanced physical mechanical parameters like stiffness and elastic modulus in addition to a high resolution profile of the sample [17], but has a limited spatial sampling speed. DIC and Phase Contrast have been used to monitor isolated cardiomyocyte contraction non-invasively but through the use of advanced image correlation analysis [18]. Each of these techniques has their own advantages and limitation and together provides complementary information that can be exploited in multimodal setups [19].

In the present article, the dynamic quantitative phase profiles of beating cardiomyocytes, which are proportional to the optical path delay profile of the cell, are reconstructed from holograms that are captured through digital holographic microscopy (DHM) [20-23]. The beating activities of cardiomyocytes, and contraction and relaxation profiles are derived from the reconstructed quantitative phase image. In addition, other characteristic parameters used to categorize phenotypes [3, 24] such as rising time, falling time, peak width, and frequency are analyzed. These parameters are valuable for the analysis of drug candidates' effects on cardiomyocytes. Other techniques usually rely on thresholding, derivative and curve fitting techniques to acquire the aforementioned parameters [3, 9].

In the present work, we analyze the dynamic beating profile of cardiomyocytes obtained by DHM using two proposed methods, either by monitoring the average or the variance information of imaged cells. We also quantify contraction and relaxation movement by analyzing the difference between two successively acquired DHM quantitative phase images. From our experimental results, we propose automated procedures for multiple parameters recording on cardiomyocytes dynamics imaged by DHM for a new methodology in drug toxicity screens.

2. Materials and Methods

2.1 Cell Culture and Imaging

iCell cardiomyocytes (human induced pluripotent stem (iPS) cell-derived cardiomyocytes) obtained for Cellular Dynamics Int. (Madison, WI) were culture according to the manufacturer's indication and grown for 14 days before recording. Measurements were achieved in a Chamlide WP incubator system for 96-well plate (LCI, South Korea) set at 37°/5% $C0_2$ with high humidity.

DHM images were acquired in an off-axis configuration on a commercially available DHM T-1001 from LynceeTec SA (Lausanne, Switzerland) equipped with a motorized xy stage (Märzhäuser Wetzlar GmbH & Co. KG, Wetzlar, Germany, ref. S429). Images were recorded using a Leica 20×/0.4 NA objective (Leica Microsystems GmbH, Wetzlar, Germany, ref. 11566049). Time-lapse images were acquired at 10 Hz for 1 minute.

2.2 Label-free Digital Holographic Imaging

DHM has been studied for applications in the field of cell biology, including automated cell counts, recognition, classification, three-dimensional tracking, and discrimination between physiological and pathophysiological states [25-32]. Briefly, DHM [20-23] is a label-free interferometric microscopy technique which provides a quantitative measurement of the optical path length. It is a two-step process where a hologram consisting of an interference pattern is first recorded on a digital camera and the quantitative phase images are reconstructed numerically using a specific algorithm [20]. With current computer power, the reconstruction process can be achieved on-the-fly at a speed of 100 image reconstruction per second. The quantitative phase images are related to the optical path difference (OPD), expressed in terms of physical properties as:

$$OPD(x,y) = d(x,y) \times \left[n_c(x,y) - n_m \right], \tag{1}$$

where $d(x,y)$ is the cell thickness, $n_c(x,y)$ is the mean intracellular refractive index integrated along the optical axis at the (x,y) position and n_m is the refractive index of the surrounding culture medium. Simply, Eq (1) means that the OPD signal is proportional to both the cell thickness and the intracellular refractive index, a property linked to the protein and water content of the cells [33-35]. DHM systems generally use a low intensity laser as a light source for specimen illumination and a digital camera to record the hologram. Here, the 684 nm laser source delivers roughly 200 $\mu W/cm^2$ at the specimen plane — that is some six orders of

magnitude less than intensities typically associated with confocal fluorescence microscopy. With that amount of light, the exposure time is only 400 µs. An extensive quality control of DHM can be found in [36]. The schematic of the off-axis DHM is shown in Fig. 1.

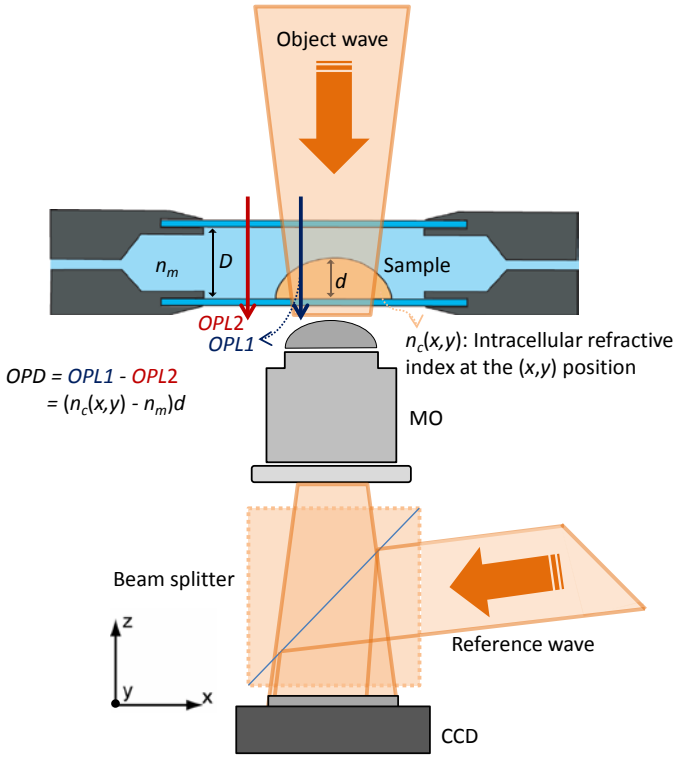

Fig. 1. The schematic of the off-axis digital holographic microscopy (DHM).

3. Automated Multi-Parameter Measurement on Cardiomyocytes Dynamics using DHM

For the quantitative analysis of cardiomyocyte dynamics, we calculated the beating activity using two alternative methods, averaged optical path difference (OPD) images and variance of OPD images. The contraction and relaxation feature of cardiomyocyte were also measured using the proposed automated procedure. Figure 2 shows two OPD images of cardiomyocytes reconstructed from holograms. The high similarity between the two images highlights the need for advanced analysis to quantify the beating dynamics.

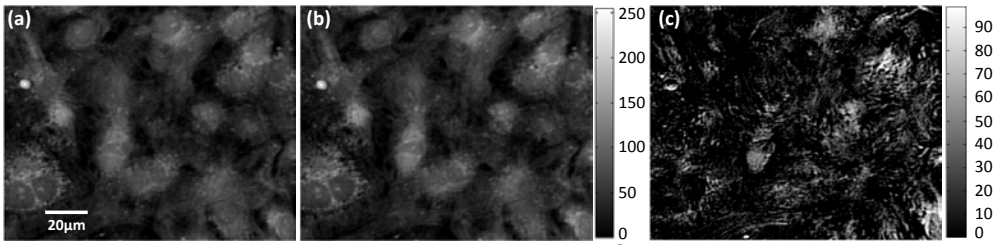

Fig. 2. The optical path difference (OPD) [nm] images of cardiomyocytes captured at different times (among total 540 frames). (a) Cardiomyocyte OPD image at the minimum of peaks. (b) Cardiomyocyte OPD image at the maximum of peaks. (c) The difference image between (a) and (b).

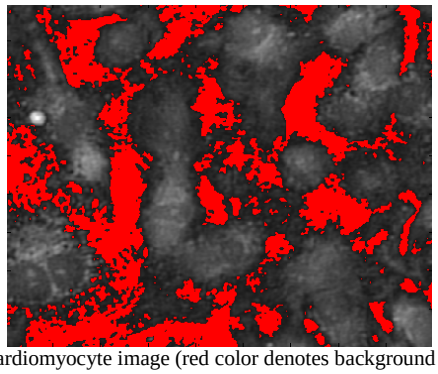

Fig. 3. Threshold cardiomyocyte image (red color denotes background after thresholding).

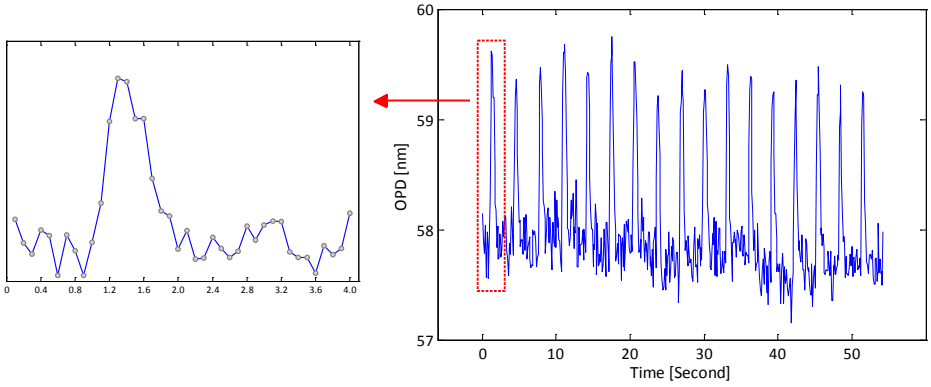

Fig. 4. Beating activity of cardiomyocyte (inset shows a single beat).

3.1 Cardiomyocytes Beating Profile Measurement using Averaged OPD Images

The beating profile of cardiomyocytes was briefly calculated by thresholding the cardiomyocyte OPD images with a threshold value of 10% of the maximum OPD signal and then the thresholded images were averaged. The threshold value is used to restrain the effect of noise. This process is described by the following equation:

$$\overline{opd}^{(i)} = average(opd\_thresh(x,y)^{(i)}),$$

$$with\ opd\_thresh(x,y)^{(i)} = \begin{cases} opd(x,y)^{(i)} & if\ opd(x,y)^{(i)} \geq \max(opd(x,y)^{(i)}) \times 0.10 \\ 0 & if\ opd(x,y)^{(i)} < \max(opd(x,y)^{(i)}) \times 0.10 \end{cases} \quad (2)$$

where $\overline{opd}^{(i)}$ is the average value of i^{th} OPD image after thresholding, $opd\_thresh(x,y)^{(i)}$ is the OPD value at location of (x,y) on the i^{th} thresholded cardiomyocyte image, $opd(x,y)$ is the OPD value at location of (x,y) for the i^{th} cardiomyocyte image in optical path difference while $1 \leqq x \leqq M$, $1 \leqq y \leqq N$ (M and N are the size of cardiomyocyte OPD image), $max(opd(x,y))^{(i)}$ means the maximum value of the i^{th} cardiomyocyte image. One of the thresholded cardiomyocyte images obtained with this method is given in Fig. 3. In addition, the beating profile with the capture time of cardiomyocytes resulted from this method is showed in Fig. 4 including a small inset with a zoom on a single beating pattern. It is noted that the beating activity of cardiomyocytes is obvious (short peaks of high amplitude). Moreover, the beating activity of cardiomyocytes with different threshold settings is presented in Fig. 5. It can be seen from Fig. 5 that the beating profiles of cardiomyocytes are approximately the same even though the

resulted OPD values are a slightly different. However, it can be expected that the final results will be very similar because the multiple parameters we want to measure only depend on the beating profile of cardiomyocytes [see Table 1 and Fig. 7]. Since these beating profiles under different threshold values are similar, the values of multiple parameters will be also similar. In other words, changing the threshold value will not strongly affect the final parameter data.

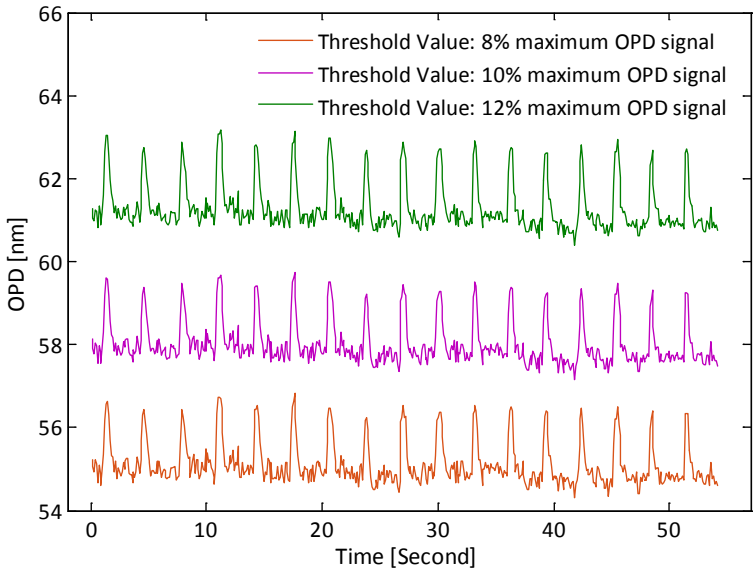

Fig. 5. Beating activity of cardiomyocyte under different threshold values.

Then, multiple parameters including amplitude, rising time, falling time, IBD_{50}, IBD_{10}, rising/falling slope, beating rate and beating period based on beating profile in Fig. 4 were derived. These parameters are described in Table 1 [2].

Table 1. Characteristic Parameters of Cardiomyocyte.

Parameter	Definition
Amplitude	Value difference from each positive peak to the following negative peak (Amplitude=Amp_{max} – Amp_{min}) [see Fig. 7]
Rising time	The time elapsed from Amp_{20} to Amp_{80} (=T_3–T_1) [see Fig. 7]
Falling time	The time elapsed from Amp_{80} to Amp_{20} (=T_6–T_4)[see Fig. 7]
IBD_{50}	The time elapsed for two points compose one Amp_{50} (=T_5–T_2) [see Fig. 7]
IBD_{10}	The time elapsed for two points compose on Amp_{10} (=T_7–T_0) [see Fig. 7]
Rising/ Falling slope	The change of increased/decreased amplitude over the time course between Amp_{80} and Amp_{20} (=Amp_{80} – Amp_{20}) [see Fig. 7]
Beating rate	The total number of positive/negative peaks in 1 minute (= total number of positive peaks/total time)
Beating period	The time between two adjacent positive and/or negative peaks (= the time of i_{th} positive peak – the time of $(i\text{-}1)_{th}$ positive peak)
Frequency	The number of beating period per second (= total number of beating period/total time)

In order to measure the above-defined parameters, peaks are detected by applying the first derivative technique to the original data curve in Fig. 4 and finding locations where the first derivative values are zeros. The detected peaks based on cardiomyocytes beating profile are given in Fig. 6(a).

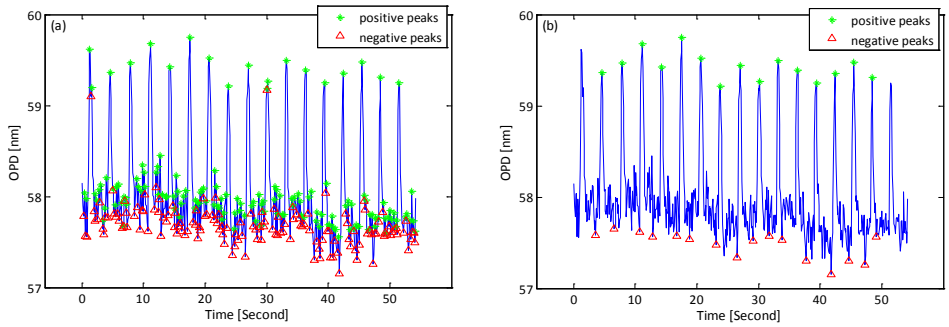

Fig. 6. Detected peaks in beating profile of cardiomyocytes.
(a) Detected peaks on raw data. (b) Filtered peaks based on results of (a).

It can be noted from Fig. 6(a) that many peaks including false peaks are detected. As a sorting process, positive peaks with values below a threshold and the negative peaks with values above a threshold are removed. This threshold can be automatically determined with Otsu's method [37] by using all of the positive peaks detected in Fig. 6(a). In addition, the minimum negative peak between two neighbor positive peaks is extracted and then the maximum positive peak between two neighboring negative peaks is selected. This process reduces some inappropriate peaks and results in appropriate peaks for each beating period as shown in Fig. 6(b).

Consequently, the beating profile between two adjacent negative peaks considered as one beating period is extracted [see Fig. 7]. It is noted that the beating periods calculated between two negative peaks is approximately equal to that between two positive peaks. At the same time, the extracted beating profile for each beating period can be fitted with polynomials of degree 9 in a least-square criterion. The degree of 9 is reached by examining polynomials of up to degree 9 (up to degree 9 because data samples among some beating profiles are around 10) for fitting the data based on the final fitting errors. The fitted polynomial with degree of 9 is described with the following equation:

$$f(x) = \sum_{i=1}^{10} a_i x^{10-i} , \tag{3}$$

where x represents the sample point on each beating period and a_i which is the coefficient of polynomial are obtained with least-square criterion based on sample points. The average absolute error for each sample point (absolute error between actual and fitted point) is measured to be 0.19. One of the fitting polynomial curves and the measured parameters are given in Fig. 7.

With the fitted polynomials curves, the amplitude value defined in Table 1 can be calculated as the maximum value minus the minimum value on the fitted curve. Thus, the corresponding time (unit is second) in x axis for Amp_{10}, Amp_{20}, Amp_{50}, Amp_{80} [see Fig. 7] can be also computed by solving the fitted polynomial equation. Then, all of the above mentioned parameters are measured for each individual beating period and a population average with coefficient of variation, (cv=standard deviation/average value, a parameter often used in high-throughput screening) is computed as shown in Table 2. The pre-mentioned values of multiple parameters are measured based on fitting a curve between two negative peaks as it allows to isolate a full beating pattern and better fit rising/falling time and amplitude, also IBD can only be measured if a full beat is present in the analyzed period. However, as shown in Fig. 5, the detected positive peaks tend to be more stable and less noisy, thus we also measured the beating period defined as the time between two adjacent positive peaks and found similar results (2.93/(sd=0.10 seconds), compared to 2.94/0.10 seconds).

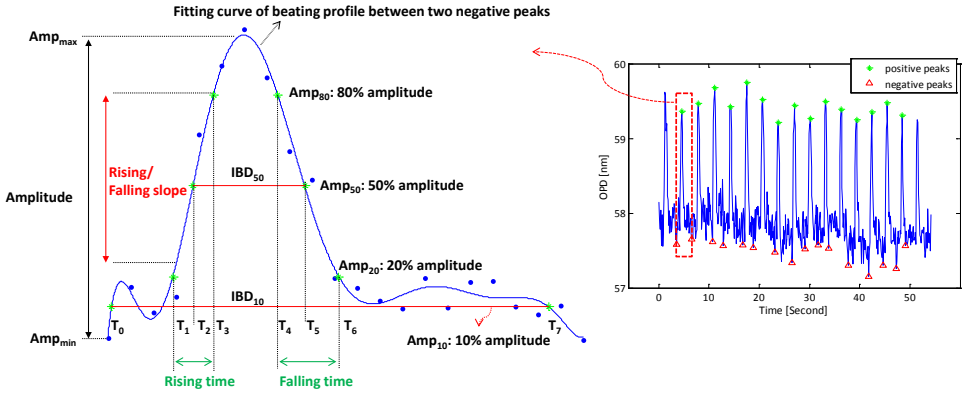

Fig. 7. Illustration of the fitted curves with parameters within one beating period on cardiomyocytes beating profile.

Table 2. Measured Values for Multiple Parameters on Cardiomyocytes Beating Profile.

Multi-parameter	Values (mean/cv)
1: Amplitude:	2.05/0.30
2: Rising time:	0.58/1.05 (seconds)
3: Falling time:	0.86/0.69 (seconds)
4: IBD_{50}:	0.79/0.33 (seconds)
5: IBD_{10}:	2.94/0.19 (seconds)
6: Rising/Falling slope:	1.19/0.30
7: Beating rate:	21.86/0
8: Beating period:	2.94/(sd=0.10 seconds)
9: Frequency	0.34/0

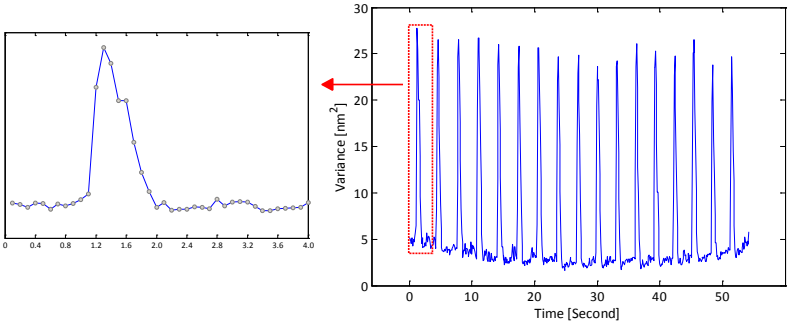

Fig. 8. Measured beating profile with variance information (inset shows a single beat).

3.2 Cardiomyocytes Beating Profile Measurement using Variance of OPD Images

An alternative way to derive the beating profile of cardiomyocytes which is less sensitive to noise (originating from shot noise, speckle and contribution of out-of-focus structures), but requires more computer resources is to measure the variance of each OPD image after the temporal mean of the image stack is subtracted. This method is illustrated by Eq. (4):

$$\delta_{\text{opd}}^{(i)} = variance\left[opd(x,y)^{(i)} - \overline{opd}_{temp} \right], \tag{4}$$

where $opd(x,y)^{(i)}$ is the i^{th} OPD image, while $1 \leqq x \leqq M$ and $1 \leqq x,y \leqq N$ (M and N are the size of cardiomyocyte OPD image), $\delta_{\text{opd}}^{(i)}$ represents the variance of the i^{th} cardiomyocyte image

after temporal mean subtracted and $\overline{opd}_{temp}$ is the temporal mean which is calculated as the mean value of the image stack in the temporal dimension. The beating profile measured with this method is showed in Fig. 8. Compared to the previous analysis method (Fig. 6), this approach is more stable and less sensitive to noise (changes in the absolute value of the OPD signal).

Similar with the previous method, the peaks in Fig. 8 can be detected using the first derivative property [see Fig. 9(a)]. In addition, the positive and negative peaks are screened with a threshold value obtained by Otsu's method [37]. Consequently, the minimum negative peak between two neighboring positive peaks and the maximum positive peak between two neighboring negative peaks are selected [see Fig. 9(b)].

The beating profile within one beating period (between two negative peaks) can be individually extracted and is fitted with polynomial equation of degree 9 in a least-square error sense as that in Fig. 7. The average absolute error for each sample point is measured to be 2.0359. Consequently, the same parameters as in the previous method can be measured and the corresponding mean and coefficient of variation (cv) are given in Table 3. The measured parameters are in excellent agreement with the literature [15].

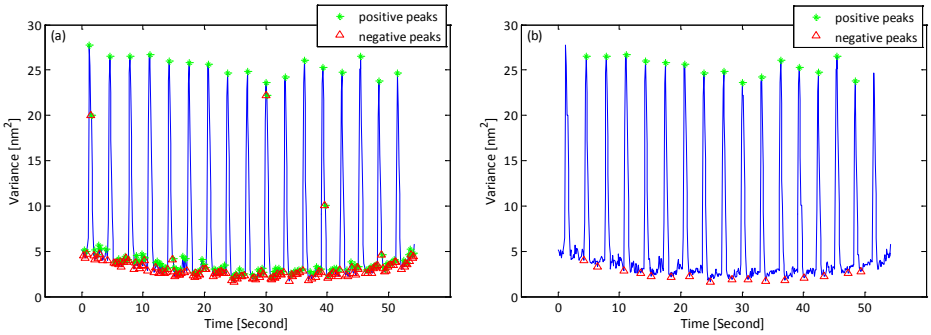

Fig. 9. Detected peaks on cardiomyocyte beating profile. (a) Detected multiple peaks. (b) Detected multiple peaks with some false peaks removed.

Table 3. Measured Multiple Parameter on Cardiomyocyte Beating Profile.

Multi-parameter	Values (mean/cv)
1: Amplitude:	23.06/0.17
2: Rising time:	0.45/0.98 (seconds)
3: Falling time:	0.26/1.04 (seconds)
4: IBD50:	0.66/0.23 (seconds)
5: IBD10:	2.30/0.25(seconds)
6: Rising/Falling slope:	13.83/0.17
7: Beating rate:	21.91/0
8: Beating period:	2.93/(sd=0.10)
9: Frequency	0.34/0

3.3 Cardiomyocytes Contraction and Relaxation Measurement

In order to observe the contraction and relaxation feature of cardiomyocyte, each captured image in the temporal stack is subtracted from the following one and then the spatial variance of the OPD is measured thus quantifying the amount of spatial displacement between successive frames (the cells used here are the same as those showed in Fig. 2). The resulting image contains cardiomyocytes contraction and relaxation information (both indicated by an increase in the temporal variance signal). Two of the subtracted images are shown in Fig. 10

where Figs. 10(a) and 10(b) are different images at the minimum and maximum of a beat, respectively. The beating profile with contraction and relaxation information of cardiomyocyte is given in Fig. 11(a), where one higher peak is for contraction and the neighboring lower peak is for relaxation. Then, the peaks can be detected with the first derivative criterion (locations where the first derivative values are zeros). Similarly, positive peaks for contraction can be properly extracted with Otsu's thresholding algorithm by using all of the detected positive peaks. Next, a maximum peak between two neighboring contraction peaks is chosen as a positive peak for relaxation. Consequently, the inappropriate peaks can be removed. The resulted curves from Fig. 11(a) with peaks indicated are given in Fig. 11(b).

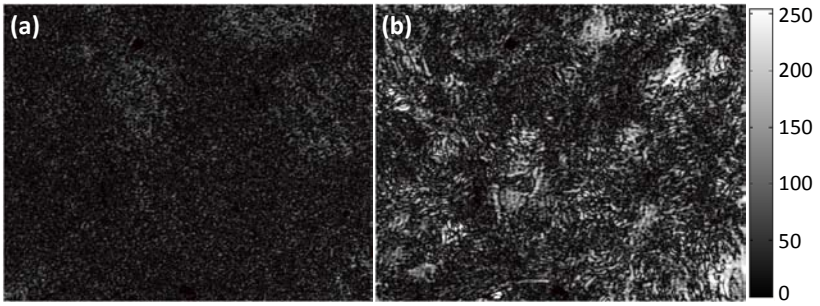

Fig. 10. Illustration of the difference images. (a) Different image at the minimum of a beat. (b) Different image at the maximum of a beat.

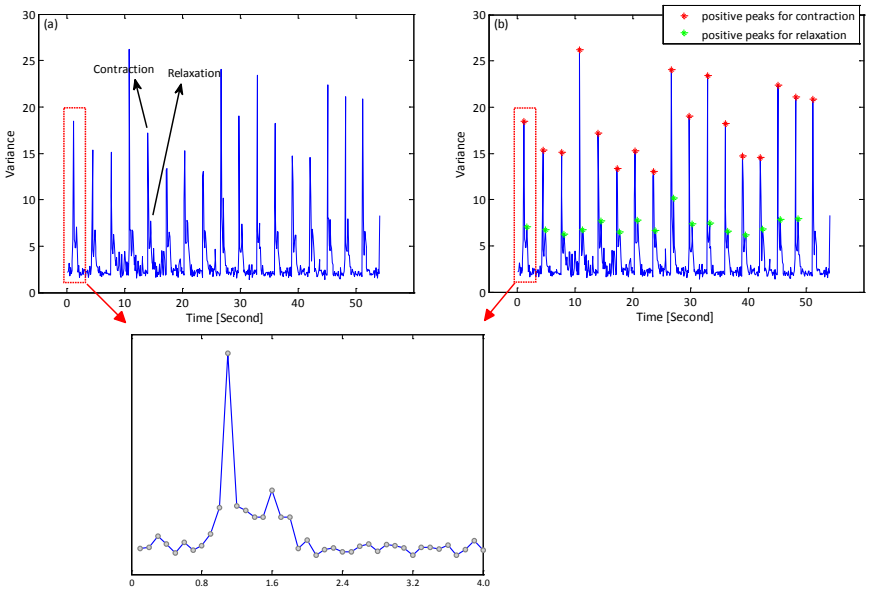

Fig. 11. Cardiomyocytes beating profile with contraction and relaxation information. (a) Raw data of cardiomyocytes beating profile. (b) Cardiomyocytes beating profile with contraction and relaxation peaks indicated (inset shows a single beat with contraction and relaxation peaks).

Finally, the beating rate, beating period and frequency for cardiomyocytes contraction and relaxation can be measured based on the detected positive peaks that include contraction and relaxation peaks. In addition, the time between the cardiomyocytes contraction and the

following relaxation can also be calculated with the detected peaks in Fig. 11(b). These measured data are given in Table 4. It is noted from Tables 1, 2, and 3 that the three methods can result in similar values for beating rate, beating period and frequency by using the same cardiomyocyte image sequence.

Table 4. Measured Parameters on Cardiomyocyte Contraction and Relaxation Curve.

Multi-parameters		Values (mean/cv)
Contraction	Beating rate:	21.71/0
	Beating period:	2.93/(sd=0.08)
	Frequency	0.34/0
Relaxation	Beating rate:	20.84/0
	Beating period:	3.05/(sd=0.49)
	Frequency	0.32/0
Time between contraction and the following relaxation		0.41/0.14

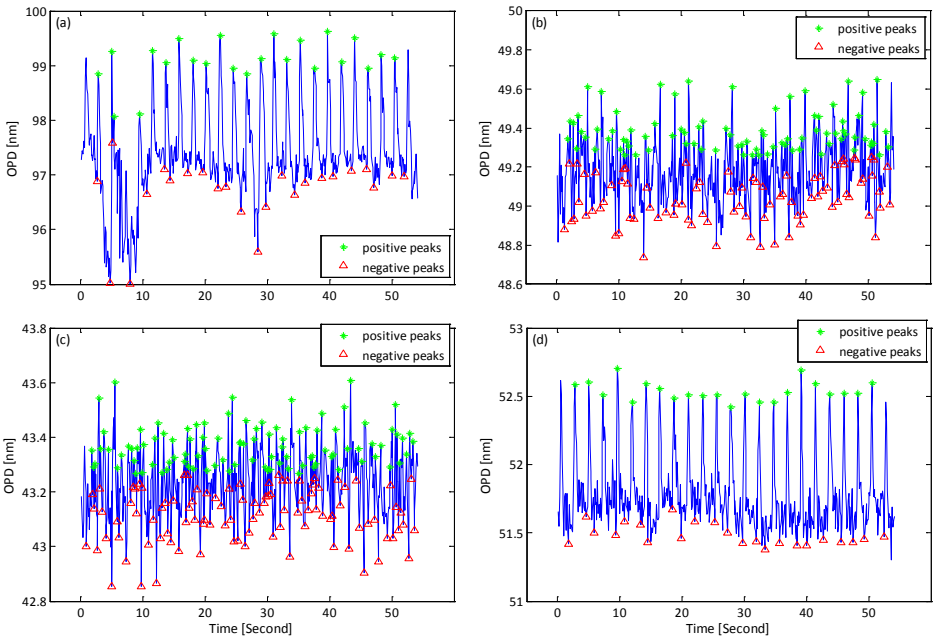

Fig. 12. Detected peaks based on four more cardiomyocyte sequences with the method in the Section 3.1. (a) Cardiomyocyte image sequences acquired with difficult conditions. (b), (c), and (d) "noise-free" recordings (i.e. no debris interfering with the measurement) similar to the previous recording.

Four more cardiomyocyte image sequences were analyzed in order to show the generality of the proposed methods. Among these image sequences, one of them is acquired with difficult conditions which mean having severe disturbance (a few out-of-focus debris are flowing through the field of view during the acquisition) while the other sequences are comparable in quality to the one presented previously. Four image sequences with peaks detected using the first (Section 3.1), second (Section 3.2) and third (Section 3.3) methods are given in Fig. 12, Fig. 13 and Fig. 14 respectively where Fig. 12 (a), Fig. 13 (a) and Fig. 14 (a) are from image sequences under tough/difficult conditions. It should be noted from these figures that our proposed method can detect all of the peaks, even in image sequences with debris interference. However, we found that the first method generated many noisy peaks in difficult conditions (1^{st} image sequence) which make the parameter measurement not accurate. On the other hand,

the second and third methods are more stable to analyze these image sequences even those obtained under difficult conditions. Consequently, all of the needed multi-parameters can be measured based on these images, therefore proving the robustness of the analysis algorithm.

Finally, the mean value of each of the parameter described in the first (Section 3. 1), second (Section 3. 2) and third (Section 3. 3) methods is measured based on all the five sequences used previously. The measured mean values for the three methods are given in Table 5, Table 6, and Table 7, respectively.

The combined measurements show the robustness of the proposed algorithm and how they allows quantify important cardiomyocyte dynamic parameters that can be used to screen compounds cytotoxic effects. The beating profile contains more information than can be obtained by electrophysiology or fluorescence imaging as it integrates the effect of all the ion-channel involved and thus offer a signature that can be used to predict the effect of specific compounds. For instance inhibitors of hERG channel (the main class of channels assessed in cardio safety, which are involved in repolarization current) all results in a similar profile [7]. In addition, due to the non-invasive aspect of the measurements, both short-term and long-term effects of the monitored compounds can be assessed with DHM.

Table 5. Measured Values for Multiple Parameters on Cardiomyocytes Beating Profile on five sequences

Multi-parameter	Values (mean/cv)
1: Amplitude:	0.85/1.50
2: Rising time:	0.62/1.37 (seconds)
3: Falling time:	0.85/0.99 (seconds)
4: IBD_{50}:	0.44/0.50 (seconds)
5: IBD_{10}:	2.44/0.45 (seconds)
6: Rising/Falling slope:	0.51/1.52
7: Beating rate:	71.14/0.81
8: Beating period:	0.95/ (sd=0.84 seconds)
9: Frequency	1.16/0.83

Table 6. Measured Multiple Parameter on Cardiomyocyte Beating Profile on five sequences

Multi-parameter	Values (mean/cv)
1: Amplitude:	40.01/1.21
2: Rising time:	0.57/0.86 (seconds)
3: Falling time:	0.43/1.13 (seconds)
4: IBD50:	0.79/0.65 (seconds)
5: IBD10:	2.35/0.38(seconds)
6: Rising/Falling slope:	24.00/1.21
7: Beating rate:	34.48/0.36
8: Beating period:	1.98/(sd=0.83)
9: Frequency	0.55/0.37

Table 7. Measured Parameters on Cardiomyocyte Contraction and Relaxation Curve on five sequences.

Multi-parameters		Values (mean/cv)
Contraction	Beating rate:	28.52/0.16
	Beating period:	2.19/0.19
	Frequency	0.45/0.16
Relaxation	Beating rate:	28.52/0.17
	Beating period:	2.22/0.31
	Frequency:	0.45/0.18
Time between contraction and the following relaxation		0.59/0.62

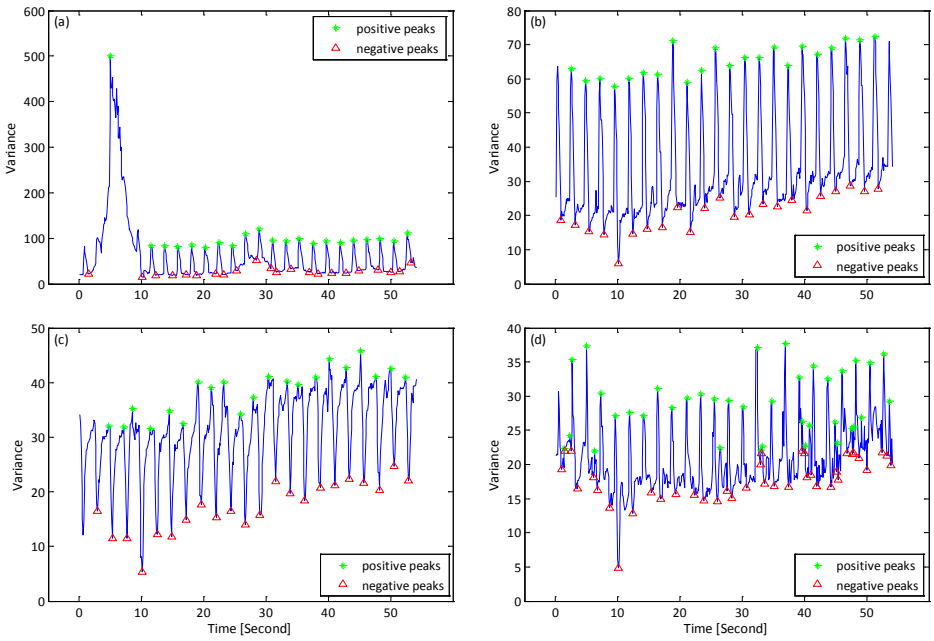

Fig. 13. Detected peaks based on four more cardiomyocyte sequences with the method in the Section 3.2. (a) cardiomyocyte image sequences acquired with difficult conditions. (b), (c), and (d) "noise-free" recordings (i.e. no debris interfering with the measurement) similar to the previous recording.

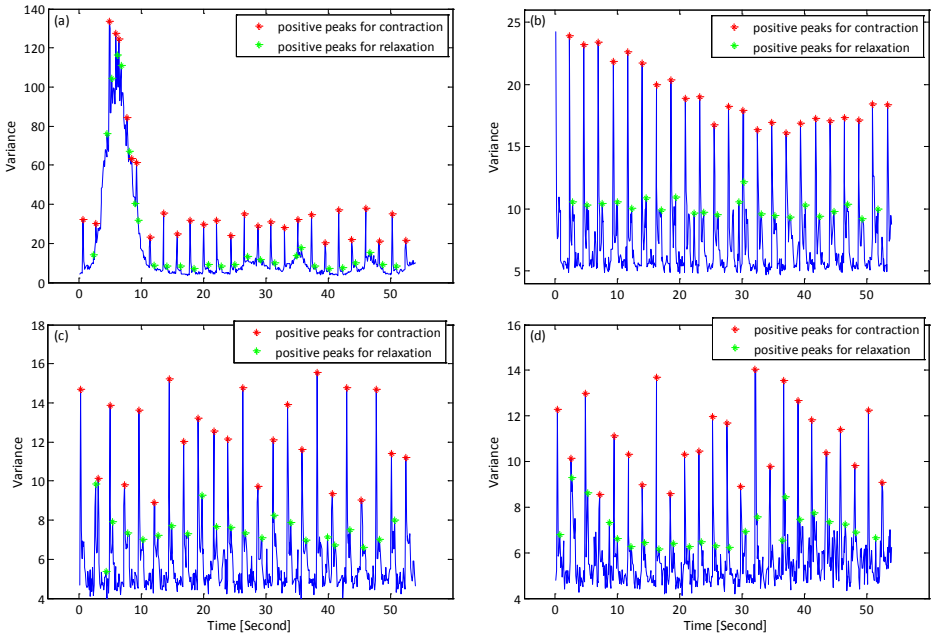

Fig. 14. Detected peaks based on four more cardiomyocyte sequences with the method in the Section 3.3. (a) cardiomyocyte image sequences acquired with difficult conditions. (b), (c), and (d) "noise-free" recordings (i.e. no debris interfering with the measurement) similar to the previous recording.

4. Conclusions

In this paper, for the first time, human cardiac muscle cells' dynamics and their spontaneous beating rates are quantitatively explored through the fusion of digital holography microscopy and information processing algorithms. We demonstrate the suitability of DHM for monitoring and quantifying the beating function of cardiomyocytes and automatically measuring multiple parameters of cardiomyocytes based on the quantitative phase profiles acquired with DHM. The proposed method can be rapid, noninvasive and effective and allows for automated analysis between normal cardiomyocyte dynamics and all other abnormal activities. We believe that our automated non-invasive measurement procedures can open new perspectives for cardiotoxicological screening or profiling of candidate molecules in preclinical drug discovery and safety testing programs.

Acknowledgments

This research was supported by Basic Science Research Program through the National Research Foundation of Korea (NRF) funded by the Ministry of Education, Science and Technology (NRF-2013R1A2A2A05005687) and Commission for Technology and Innovation (CTI) of the Swiss Confederation (grant No. 12669.1 PFLS-LS)